Metalurgi (2024) 3: 151-158

METALURGI
Majalah Ilmu dan Teknologi
p-ISSN 0126-3188 | e-ISSN 2443-3926
ejurnalmaterialmetalurgi.lipi.go.id

INVESTIGATION OF FAILURE MECHANISMS IN U-BEND TUBES OF SHELL-AND-TUBE HEAT EXCHANGERS

Mochamad Achyarsyah[a,*], Kus Hanaldi[a], Wiwik Purwadi[a], Gita Novian Hermana[b], Ari Siswanto[b], Cecep Ruskandi[b], Muhammad Rizki Gorbyandi Nadi[b]

[a]Department of Foundry Engineering, Bandung Polytechnic for Manufacturing
[b]Department of Advanced Materials Engineering, Bandung Polytechnic for Manufacturing
Kanayakan No. 21, Bandung, Jawa Barat, Indonesia 40135
*E-mail: achyarsyah@polman-bandung.ac.id

Received: 110-09-2025, Revised: 05-01-2025, Accepted: 08-01-2026

Abstract

The U-bend tubes of a shell-and-tube heat exchanger made of SA-234 Grade WPB carbon steel failed prematurely within 14 days after replacement and welding. This study investigates failure mechanisms through an integrated failure analysis that includes visual inspection, dye penetrant testing, chemical composition analysis, hardness measurements, and microstructural characterization. The results reveal that the tube contained 0.324 wt.% C, exceeding the maximum limit specified by the standard, which promoted the formation of Widmanstätten ferrite and reduced toughness. The welded joint exhibited multiple defects, including porosity and lack of fusion, which acted as stress concentration sites. Hardness measurements showed average values of 205 HV in the weld metal, 199 HV in the HAZ (heat-affected zone), and 184 HV in the base metal. Under operating conditions of 275 °C and 58.48 barg, these defects progressively opened, leading to fluid leakage. The escaping high-pressure fluid accelerated erosion-corrosion, as evidenced by oxygen-rich corrosion products detected by EDS analysis. The findings demonstrate that the combined effects of material non-compliance, poor welding quality, and unfavorable microstructural evolution governed the premature failure. This study provides quantitative insights to improve welding practices and material selection, thereby enhancing the reliability of U-bend tubes in shell-and-tube heat exchangers.

Keywords: *U-bend tube, failure analysis, heat exchangers, steel, widmanstätten*

1. INTRODUCTION

Shell-and-tube heat exchangers play an essential role in a wide range of industries, including chemical, thermoelectric power generation, oil refining, and mineral processing [1]-[3]. These exchangers are widely used because they reduce energy consumption by transferring heat between fluids at different temperatures. Among the critical components of shell-and-tube heat exchangers, the shell-and-tube themselves are essential for facilitating heat transfer between two fluids; one fluid flows through the tubes, while another fluid flows across the shell side [4].

Failures in shell-and-tube heat exchangers pose significant challenges to the industry, despite regular maintenance being scheduled to prevent such issues. Chemical corrosion, SCC (stress corrosion cracking), and mechanical failures, or a combination of these factors, are the leading causes of failure in shell-and-tube heat exchangers [5]-[8]. Edi Purnomo et al. reported that the failure of the U-bend in the heat exchanger was caused by welding defects and corrosion due to oxygen reactions, exacerbated by cyclic operational stresses [2]. Another study by Rezaei et al. reported that erosion-corrosion, caused by solid particles generated during catalysis, affected the

DOI: 10.55981/metalurgi.2024.775

Metalurgi is Sinta 2 Journal (https://sinta.kemdikbud.go.id/journals/profile/3708) accredited by Ministry of Education, Culture, Research, and Technology, Republic Indonesia

performance of heat exchangers and led to tube failure [9]. Panahi et al. also investigated failures in shell-and-tube heat exchangers caused by crevice corrosion between the external surface of the tubes and the tube sheet [6]. Previous studies reported that welded joints are particularly susceptible to deterioration mechanisms such as pitting corrosion, SCC, and welding defects [10]-[11]. As a result, cracks and other defects may form in the welded joints, potentially leading to failure of the shell-and-tube heat exchanger.

Although numerous investigations have addressed failures in shell-and-tube heat exchangers, most studies focus on individual failure mechanisms in isolation, such as corrosion or welding defects. A systematic correlation between material composition, welding quality, microstructural evolution, and operational conditions, especially in cases of premature failure after repair welding, remains insufficiently explored.

Therefore, this study aims to investigate the root cause of failure at the welded joint on the U-bend tube in a shell-and-tube heat exchanger that failed during operation by correlating material properties, joining processes, microstructural features, and service conditions. Furthermore, this study seeks to establish an integrated failure mechanism, demonstrating that premature failure is governed by the combined effects of material non-compliance, welding-induced defects, and unfavorable microstructural evolution under high-temperature and high-pressure operating conditions. The investigation process involves examining the failed tube and U-bend tube using a combination of visual examination, non-destructive testing, and microstructural observations. By thoroughly evaluating the failed components, identifying material degradation, and analyzing the microstructure, the root cause of failure can be determined.

2. MATERIALS AND METHODS

2.1 Material

The operating conditions on the tube side of the shell-and-tube heat exchanger in the chemical plant were 275 °C and 58.48 barg. According to the design specifications, the heat exchanger tubes were rated to withstand temperatures up to 360 °C and pressure up to 72 barg. Figure 1 shows a schematic of the failed shell-and-tube heat exchanger that was investigated in this study. The materials used for the U-bend tube are carbon steel, specifically SA-234 Grade WPB.

The first signs of leakage in several tubes were observed around 6 months after the commencement of operation. The leaking tube was subsequently replaced with a new U-bend tube and joined using GTAW (gas tungsten arc welding), with TG-S50 (Kobelco, Japan) filler metal classified under AWS A5.18 ER70S-G, with a filler diameter of 2.4 mm.

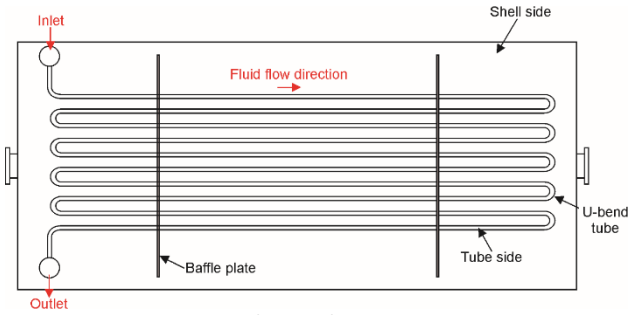

Figure 1. Schematic of the failed shell-and-tube heat exchanger

However, another leak occurred approximately 14 days after the replacement. The failed tube and its condition near the weld metal are shown in Fig. 2.

(a)

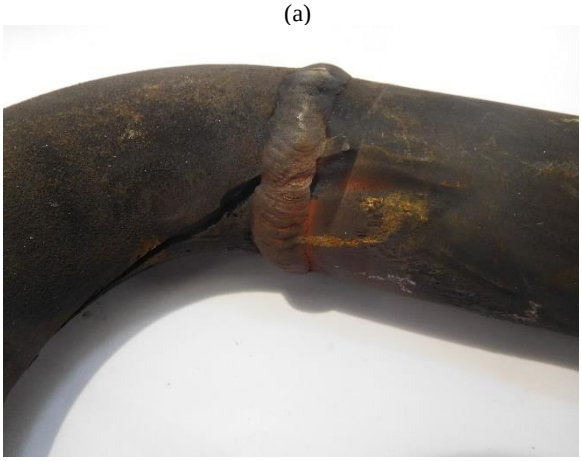

(b)

Figure 2. Photograph of the shell-and-tube heat exchanger (a) overall and (b) near the welded metal

Upon leakage, as indicated by several symptoms presented in Table 1, there was a significant drop in both the pressure inside the tube and temperature. Furthermore, the outlet temperature on the shell side also plummeted to 75.54 °C.

2.2 Method

In the present study, an investigation of all possible causes of failure was carried out through experimental analysis. Visual observations and dye penetrant testing were performed on the failed tube, and macroscopic evaluation was conducted using a stereomicroscope (Olympus SZ61, Japan). Optical emission spectrometry (OES; ARL 3460) was employed to evaluate the chemical composition of the failed tube. The failed tube was carefully cut near the weld, and the surface was cleaned to remove contaminants. Standard metallographic preparation was performed on the sample before observation under an optical microscope (OM; Olympus QX71, Japan).

Table 1. Indications of leakage in the tube during operation

Date	Time	Tube		Shell	
		P (barg)	T (°C)	Inlet T (°C)	Outlet T (°C)
30 Dec	22.11	59.01	274.81	384.42	280.66
31 Dec	10.00	59.15	274.23	384.27	280.76
	10.44	59.09	274.92	384.00	280.45
1 Jan	09.50	59.52	274.66	384.40	274.13
	10.06	55.35	271.99	384.42	235.21
	10.14	39.86	247.95	384.40	202.94
	11.00	13.99	189.80	381.06	75.54
7 Jan	09.00	59.35	276.41	384.60	282.07
	10.00	59.30	276.46	384.77	282.17
	11.00	59.19	276.34	384.73	282.04

To obtain more detailed information on chemical structure, an EDX (energy dispersive X-ray spectroscopy), which was equipped with the SEM (scanning electron microscope) Hitachi SU 3500 Japan, was utilized to observe the chemical structure of deposits. The mechanical properties of the failed tube were determined using the micro-Vickers hardness method with a universal hardness tester (Zwick Roell ZHU250CL, Germany).

3. Results and Discussion

3.1 Macroscopic Examination

Figure 3 shows the macroscopic evaluation of the failed U-bend tube after dye penetrant testing was conducted. The red areas in the image indicate defects revealed by the dye penetrant test. Several defects were observed in the failed U-bend tube. A continuous defect is observed around the joint area, as shown in Fig. 3(a). As seen from Figure 3(b), there are several holes in the outer surface of the failed tube, as shown by arrows. The formation of small holes in the outer surface of the failed tube is indicative of pitting corrosion. In the weld metal region, penetration is insufficient, as shown in Fig. 3(c). This indication refers to the condition in which the top part of the weld joint does not fuse with the base metal. These macroscopic defects indicate potential sites of stress concentration, which may serve as preferential locations for crack initiation under internal pressure and elevated operating temperatures.

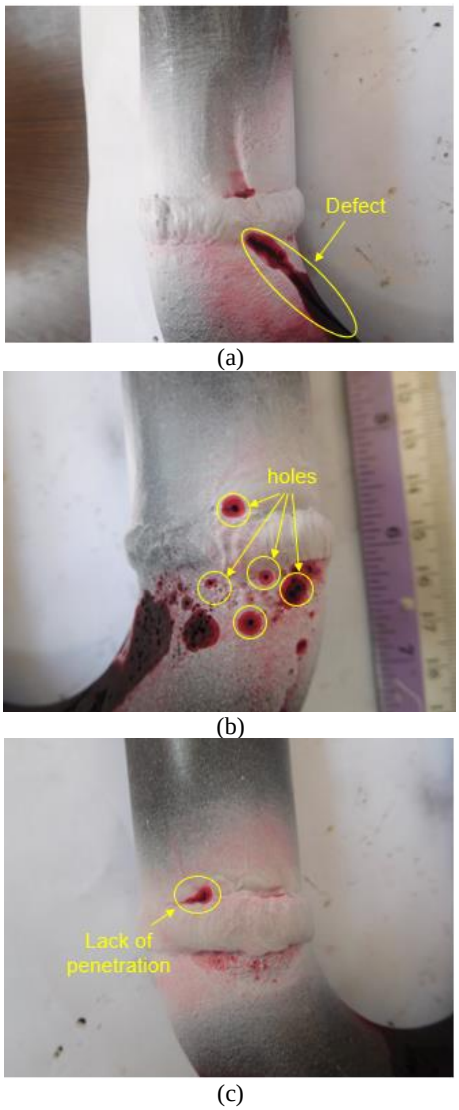

Figure 3. Macroscopic evaluation of defect types (a) continuous defect, (b) small holes, and (c) lack of penetration in the failed tube

3.2 Chemical Analysis

The chemical composition of the U-bend tube was tested using OES and compared with the standard specification of SA-234 Grade WPB. The results of the OES analysis, as shown in Table 2, indicate that the failed tube contains a carbon (C) composition exceeding 0.3 wt.%, which exceeds the carbon content specified in the standard material.

Table 2. Chemical composition of the U-bend failed tube

Element (wt.%)	Standard	Sample
C	0.300 Max	0.324
Si	0.100 Min	0.237
S	0.058 Max	0.001
P	0.050 Max	0.006
Mn	0.290-1.060	0.621
Ni	0.400 Max	0.009
Cr	0.400 Max	0.081
Mo	0.150 Max	0.020
Fe	Bal.	Bal.

Since carbon plays a vital role in microstructural transformations and the mechanical properties of steel, excessive carbon may significantly contribute to the failure of the shell-and-tube heat exchanger. The excess carbon content is significant because it promotes the formation of brittle microstructural features, such as Widmanstätten ferrite, thereby increasing crack susceptibility during service.

3.3 Hardness

The micro-Vickers hardness test was conducted to measure the hardness of the U-bend-failed tube using a 1 kg load. Measurements were taken in three different areas of the sample – the weld metal, the heat-affected zone (HAZ), and the base metal – with three indentations performed in each region. The hardness values of the failed U-bend tube are presented in Table 3. The hardness results indicate that the weld metal has the highest average hardness among the regions, although the difference is not statistically significant, with an average hardness of 205 HV. Meanwhile, the hardness testing results in the HAZ area show an average of 199 HV, whereas the base metal exhibits the lowest average of 184 HV.

Table 3. Hardness test results of the failed U-bend tube sample

Test No.	Sample		
	Weld metal	HAZ	Base metal
1	207	202	185
2	208	193	183
3	201	199	180
4	203	200	187
Average	205	199	184

3.4 Microscopic Examination

A sample was carefully cut from the welded joint of the failed U-bend tube, then ground with silicon carbide (SiC) grade 60-1500, polished with alumina paste (Al_2O_3), and etched with Nital. The morphology of the sample is divided into three distinct areas: the weld metal, the HAZ, and the base metal. Figure 4(a) shows a low-magnification overview of the weld metal and adjacent HAZ from the sample. The region adjacent to the weld metal exhibits microstructural features characteristic of the HAZ, with a gradual variation in grain size due to thermal gradients during welding.

The microstructure of the welded metal consists of evenly dispersed acicular ferrite phase and bainite throughout the welded metal, as can be seen in Fig. 4(b). The acicular ferrite can be differentiated by morphological observation because it forms a microstructure called small, non-aligned grains. The formation of the acicular ferrite microstructure may result from inclusions as a driving force for nucleation. The generation of thermal strains in the austenite phase or the formation of solute-depleted regions are the most likely mechanisms for this phenomenon [12]-[13]. A previous study also reported that the acicular ferrite microstructure on the weld metal provides an optimum combination of strength and toughness [14]. On the other hand, bainite (lath structures) is identified as a ferrite arranged in parallel positions. They can be characterized by more than two parallel lath ferrites within a single prior-austenite grain [12].

Figure 4(c) depicts the microstructure of the HAZ from the failed tube sample. Depending on the distance from the weld metal, the HAZ area can be divided into two distinct subzones: the coarse-grain HAZ (CGHAZ) and the fine-grain HAZ (FGHAZ). Several studies have reported that the peak temperature and cooling rate influence microstructural evolution in the HAZ in each subzone. Therefore, the effects of these two parameters can be correlated with the distance from the weld metal [15]-[18]. These subzones exhibit distinct mechanical and physical properties that may constitute weak points in the welded joint.

Several microstructures were observed in the base metal, as presented in Fig. 4(d). Pearlite is the dominant phase, while three distinct types of ferrite (α) can also be observed in the microstructure. The α-phase, with a plate-like or needle-like morphology, is known as α-Widmanstätten. This type of ferrite is usually undesirable because it reduces steel toughness and increases susceptibility to brittle fracture. This

structure is also classified as an unfavorable microstructure in carbon steel. The presence of Widmanstätten ferrite reduces toughness and increases susceptibility to brittle fracture, particularly under combined thermal and mechanical loading.

Other ferrite types observed in the microstructure include α-idiomorphic and α-allotriomorphic. These two types of ferrite have long been classified as transformation products of austenite, as their formation is strongly influenced by nucleation site location. In the case of α-idiomorphic, nucleation is closely associated with the presence of carbides or inclusions inside the grains [19]-[22]. On the other hand, α-allotriomorphic nucleates at the grain boundary of austenite and grows along the boundaries [23]-[24].

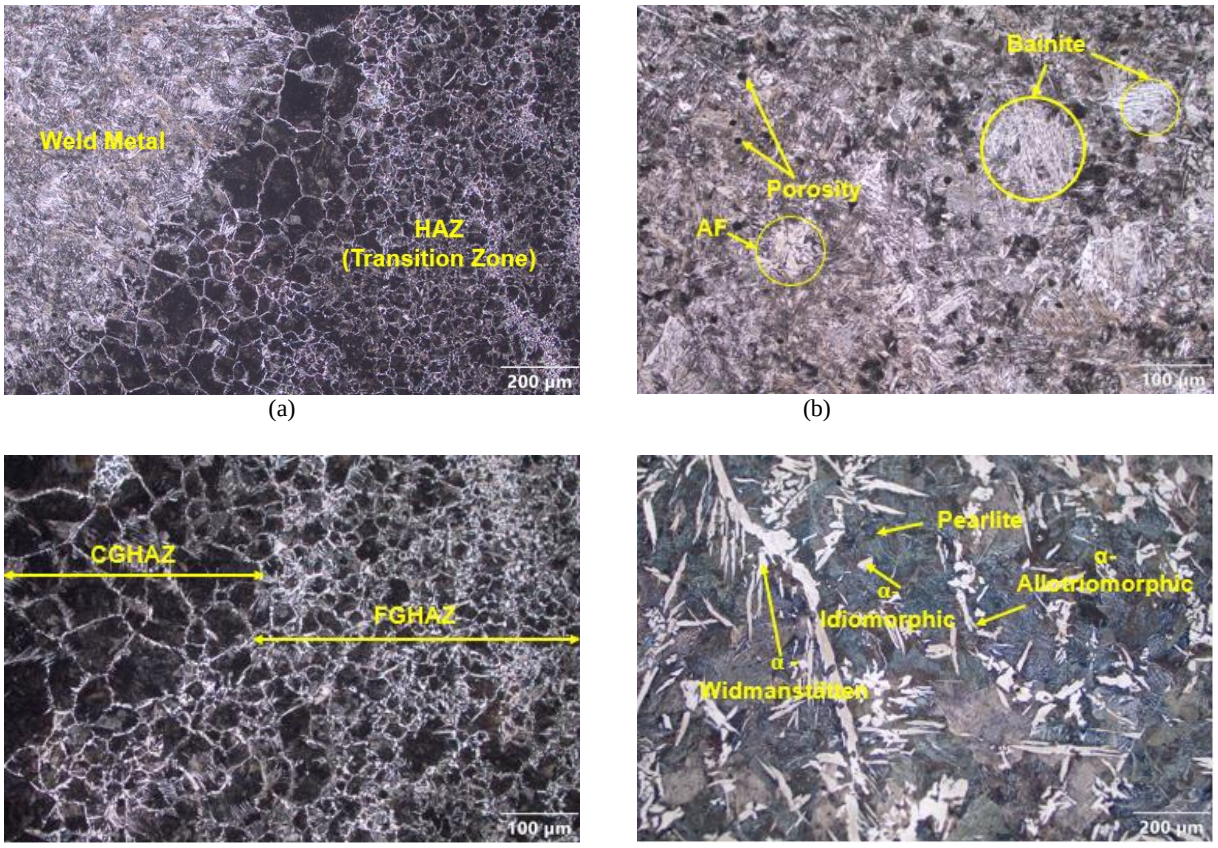

Figure 4. Metallurgical microstructure of the failed U-bend tube near the welded joint area, (a) low magnification overview of the welded joint, where the boundaries between the welded metal and HAZ are schematically indicated, (b) the weld metal, (c) the HAZ, and (d) the base metal

Figure 5 illustrates the metallurgical microstructure around the welded joint area of the failed tube. Numerous small porosities formed in the weld metal during welding, and a large porosity is present near the weld-base metal interface. Furthermore, the welding process appears to have been improperly performed, as evidenced by a lack of fusion between the weld metal and the base metal.

EDS analysis was conducted to investigate the potential for corrosion on the inner surface of the failed tube. As indicated by the white region in Fig. 6, the results revealed the existence of the oxygen (O) element. This element may react with Fe to form iron oxide, such as FeO, Fe_2O_3, or Fe_3O_4 on the surface of the failed tube. The formation of these compounds indicates that corrosion has occurred in the failed tube.

3.5 Root Causes Analysis

Owing to the complexity of the structure and operating conditions in shell-and-tube heat exchangers, several types of failure commonly occur, including corrosion and poor weld quality. Corrosion is a common cause of failure in this type of heat exchangers and is often triggered by water containing minerals or other corrosive substances. A different kind of failure that could occur in the failed tube is triggered by poor welding quality.

In this study, the chemical composition of the failed tube material does not comply with the material standard. The failed tube contains 0.324

wt.% C, which is 0.024 wt.% higher than the maximum requirements specified by the standard. Additionally, the Si content is also 0.137 wt.% higher than the standard value. These deviations may increase the tube's hardness and tensile strength. This condition may be further aggravated by the formation of Widmanstätten structures, which reduce the tube's toughness.

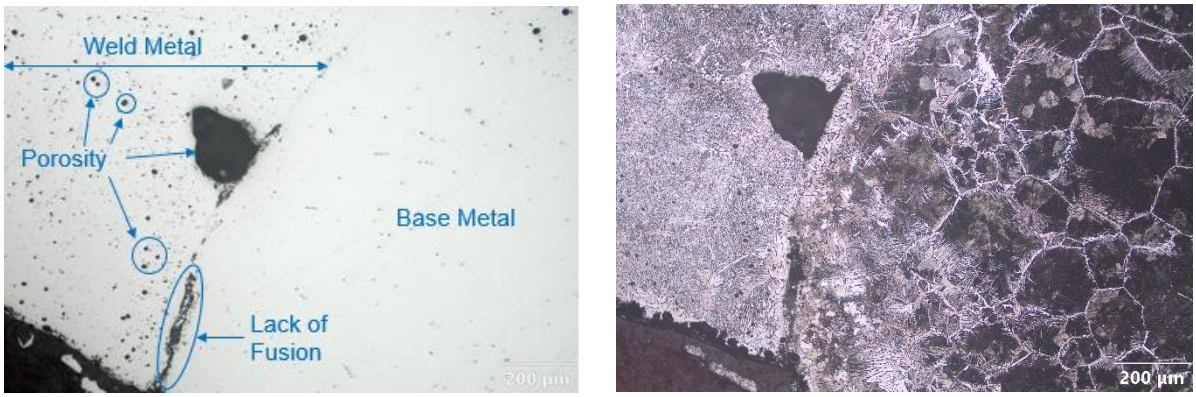

(a) (b)

Figure 5. Metallurgical microstructure of the welded joint area (a) without etching and (b) with 3% Nital etching

Welding quality is considered a primary cause of tube failure, as evidenced by multiple welding defects. These defects act as stress concentrators within the tube material. When the tube is subjected to internal loading from pressurized fluid flow and to elevated temperatures during operation, initial defects formed during welding tend to open, expand, and eventually allow fluid to leak from the tube.

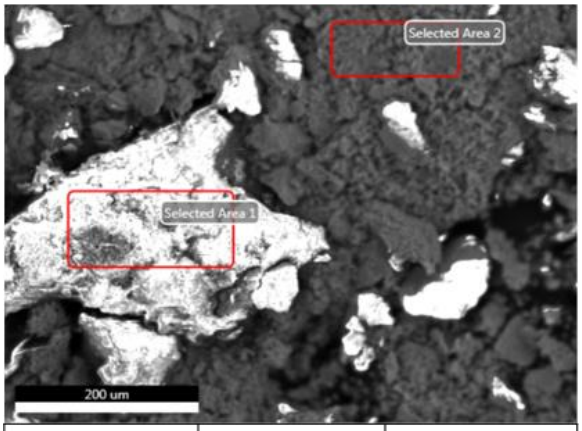

Element	wt.%	at.%
C K	48.22	63.74
O K	30.34	30.11
S K	0.28	0.14
Fe K	21.17	6.02

Figure 6. EDS results of the failed U-bend tube sample

Leakage of pressurized fluid from the tube, along with high temperatures on the shell side, promotes corrosion and erosion of the tube's outer surface. This is evidenced by the presence of oxygen on the tube surface, indicating the formation of iron oxides such as FeO, Fe_2O_3, or Fe_3O_4. Meanwhile, erosion is identified by the continuous appearance of surface defects on the tube exterior, as shown in Fig. 3(a).

Based on the combined macroscopic, chemical, mechanical, and microstructural analyses, the failure mechanism can be described as a sequential process in which material non-compliance promoted unfavorable microstructural features, welding defects acted as stress-concentration sites, and operational pressure and temperature facilitated crack opening and leakage. Subsequent erosion-corrosion further accelerated material degradation, leading to premature failure.

4. CONCLUSION

The interaction among material non-compliance, welding defects, and operational loading conditions led to the premature failure of the U-bend tube in the shell-and-tube heat exchanger. The carbon content of the tube (0.324 wt.%) exceeded the allowable limit, promoting the formation of Widmanstätten ferrite, thereby reducing toughness and increasing crack susceptibility. Welding defects, particularly porosity and lack of fusion, were identified as the primary initiation sites for failure. These defects produced localized stress concentrations that progressively opened under internal pressures of 58.48 barg and elevated operating temperatures of 275 °C. Hardness variations across the welded joint (184-205 HV) further indicate microstructural heterogeneity that contributed to mechanical instability. Following leakage, the interaction between the high-temperature fluid and the tube exterior accelerated erosion-

corrosion, as evidenced by iron oxide formation detected by EDS analysis. The findings highlight the necessity of strict control of material composition, improved welding procedures, and post-weld inspection. Future work should focus on quantitative life prediction models and process optimization for welded U-bend components operating under high-pressure and high-temperature conditions.

ACKNOWLEDGEMENT

The authors thank Yun Gemilang and Lili Hariyadi of the Materials Laboratory at Bandung Polytechnic for their assistance.

REFERENCES

[1] C. Wu, H. Yang, X. He, C. Hu, L. Yang, and H. Li, "Principle, development, application design and prospect of fluidized bed heat exchange technology: Comprehensive review," *Renewable and Sustainable Energy Reviews*, vol. 157, p. 112023, 2022. DOI:10.1016/j.rser.2021.112023.

[2] E. Purnomo, A. Wiranata, and M. A. Muflikhun, "Microstructural and mechanical characterization of u-bend economizer failures: Integrating experimental testing and CFD simulation," *Journal of Materials Research and Technology*, vol. 36, pp. 4692-4702, 2025. DOI:10.1016/j.jmrt.2025.04.178.

[3] C. R. d. F. Azevedo, F. B. Neto, S. D. Brandi, and A. P. Tschiptschin, "Cracking of 2.25 Cr-1.0 Mo steel tube/stationary tube-sheet weldment of a heat-exchanger," *Engineering Failure Analysis*, vol. 15, no. 6, pp. 695-710, 2008. DOI:10.1016/j.engfailanal.2007.06.013.

[4] L. Liu, N. Ding, J. Shi, N. Xu, W. Guo, and C.-M. L. Wu, "Failure analysis of tube-to-tubesheet welded joints in a shell-tube heat exchanger," *Case Studies in Engineering Failure Analysis*, vol. 7, pp. 32-40, 2016. DOI:10.1016/j.csefa.2016.06.002.

[5] R. T. Mousavian, E. Hajjari, D. Ghasemi, M. K. Manesh, and K. Ranjbar, "Failure analysis of a shell-and-tube oil cooler," *Engineering Failure Analysis*, vol. 18, no. 1, pp. 202-211, 2011. DOI:10.1016/j.engfailanal.2010.08.022.

[6] H. Panahi, A. Eslami, M. Golozar, and A. A. Laleh, "An investigation on corrosion failure of a shell-and-tube heat exchanger in a natural gas treating plant," *Engineering Failure Analysis*, vol. 118, p. 104918, 2020. DOI: 10.1016/j.engfailanal.2020.104918.

[7] S. Xu, C. Wang, and W. Wang, "Failure analysis of stress corrosion cracking in heat exchanger tubes during start-up operation," *Engineering Failure Analysis*, vol. 51, pp. 1-8, 2015. DOI: 10.1016/j.engfailanal.2015.02.005.

[8] Z. G. Yang, Y. Gong, and J. Z. Yuan, "Failure analysis of leakage on titanium tubes within heat exchangers in a nuclear power plant. Part I: Electrochemical corrosion," *Materials and Corrosion*, vol. 63, no. 1, pp. 7-17, 2012. DOI:10.1002/maco.201106189.

[9] M. Rezaei, Z. Mahidashti, S. Eftekhari, and E. Abdi, "A corrosion failure analysis of heat exchanger tubes operating in petrochemical refinery," *Engineering Failure Analysis*, vol. 119, p. 105011, 2021. DOI:10.1016/j.engfailanal.2020.105011.

[10] V. Korobko, A. Shevtsov, S. Serbin, H. Wen, and M. Dzida, "Impact of the type of heat exchanger on the characteristics of low-temperature thermoacoustic heat engines," *International Journal of Thermofluids*, vol. 24, p. 100953, 2024. DOI:10.1016/j.ijft.2024.100953.

[11] F. Yan, H. Lu, and S. Feng, "Numerical simulation of liquified natural gas boiling heat transfer characteristics in helically coiled tube-in-tube heat exchangers," *Frontiers in Heat and Mass Transfer*, vol. 22, no. 5, pp. 1493-1514, 2024. DOI:10.32604/fhmt.2024.055324.

[12] D. Abson, "Acicular ferrite and bainite in C–Mn and low-alloy steel arc weld metals," *Science and Technology of Welding and Joining*, vol. 23, no. 8, pp. 635-648, 2018. DOI:10.1080/13621718.2018.1461992.

[13] A. Takada, H. Terasaki, and Y. Komizo, "Effect of aluminium content on acicular ferrite formation in low carbon steel weld metals," *Science and Technology of Welding and Joining*, vol. 18, no. 2, pp. 91-97, 2013. DOI:10.1179/1362171812Y.0000000086.

[14] S. S. Babu, "The mechanism of acicular ferrite in weld deposits," *Current opinion in solid state and materials science*, vol. 8, no. 3-4, pp. 267-278, 2004. DOI:10.1016/j.cossms.2004.10.001.

[15] M. Amraei, S. Afkhami, V. Javaheri, J. Larkiola, T. Skriko, T. Björk, and X. L. Zhao, "Mechanical properties and microstructural evaluation of the heat-affected zone in ultra-high strength steels," *Thin-Walled Structures*, vol. 157, p.

107072, 2020. DOI:10.1016/j.tws.2020.107072.
[16] A. Smith, M. Asadikiya, M. Yang, J. Chen, and Y. Zhong, "An investigation of creep resistance in grade 91 steel through computational thermodynamics," *Engineering,* vol. 6, no. 6, pp. 644-652, 2020. DOI:10.1016/j.eng.2019.12.004.
[17] S. Afkhami, V. Javaheri, M. Amraei, T. Skriko, H. Piili, X. L. Zhao, and T. S. Björk, "Thermomechanical simulation of the heat-affected zones in welded ultra-high strength steels: Microstructure and mechanical properties," *Materials & Design,* vol. 213, p. 110336, 2022. DOI:10.1016/j.matdes.2021.110336.
[18] H. Zhou, Q. Zhang, B. Yi, and J. Wang, "Hardness prediction based on microstructure evolution and residual stress evaluation during high tensile thick plate butt welding," *International Journal of Naval Architecture and Ocean Engineering,* vol. 12, pp. 146-156, 2020. DOI:10.1016/j.ijnaoe.2019.09.004.
[19] C. Capdevila, F. G. Caballero, C. García-Mateo, and C. G. De Andrés, "The role of inclusions and austenite grain size on intragranular nucleation of ferrite in medium carbon microalloyed steels," *Materials transactions,* vol. 45, no. 8, pp. 2678-2685, 2004. DOI:10.2320/matertrans.45.2678.
[20] M. Y. Chen, H. W. Yen, and J. R. Yang, "The transition from interphase-precipitated carbides to fibrous carbides in a vanadium-containing medium-carbon steel," *Scripta Materialia,* vol. 68, no. 11, pp. 829-832, 2013. DOI:10.1016/j.scriptamat.2013.01.020.
[21] Y. Chi, Y. Tsai, B. Huang, and J. Yang, "Investigation of idiomorphic ferrite and allotriomorphic ferrite using electron backscatter diffraction technique," *Materials Science and Technology,* vol. 33, no. 5, pp. 537-545, 2017. DOI:10.1080/02670836.2016.1216027.
[22] T. Yokomizo, M. Enomoto, O. Umezawa, G. Spanos, and R. Rosenberg, "Three-dimensional distribution, morphology, and nucleation site of intragranular ferrite formed in association with inclusions," *Materials Science and Engineering: A,* vol. 344, no. 1-2, pp. 261-267, 2003. DOI:10.1016/S0921-5093(02)00411-2.
[23] C. Capdevila, F. Caballero, and C. García de Andrés, "Modeling of kinetics of austenite-to-allotriomorphic ferrite transformation in 0.37 C-1.45 Mn-0.11 V microalloyed steel," *Metallurgical and Materials Transactions A,* vol. 32, pp. 661-669, 2001. DOI:10.1007/s11661-001-1001-1.
[24] W. Lange, M. Enomoto, and H. Aaronson, "The kinetics of ferrite nucleation at austenite grain boundaries in Fe-C alloys," *Metallurgical Transactions A,* vol. 19, pp. 427-440, 1988. DOI:10.1007/BF02649256.